KVN Status Report 2023

Korean VLBI Network, Korea Astronomy and Space Science Institute

KVN group, Radio astronomy division

May 14, 2023

Contents

1 Introduction **5**

2 KVN System **6**

2.1 Network . . . 6
2.1.1 Array . . . 6
2.1.2 UV coverage . . . 6
2.1.3 Antenna location . . . 6
2.1.4 Array Operation Center (AOC) . . . 6
2.2 Antennas . . . 8
2.2.1 Optics and Driving performance . . . 8
2.2.2 Gain Curve . . . 9
2.2.3 Antenna beam size and Aperture efficiency . . . 9
2.2.4 Beam pattern . . . 11
2.2.5 Antenna pointing accuracy . . . 11
2.2.6 Beam alignment . . . 14
2.2.7 Skylines . . . 15
2.3 Receiver . . . 16
2.3.1 Quasi-optics . . . 16
2.3.2 Block diagram . . . 16
2.3.3 Frequency range . . . 18
2.3.4 Receiver noise temperature . . . 19
2.3.5 System temperatures with wide-band frequencies . . . 19
2.4 Digital Process . . . 20
2.4.1 Digital filter mode . . . 20
2.4.2 Signal processing mode of OCTAD . . . 21
2.4.3 Recorders . . . 22
2.4.4 Spectrometers for Single-dish observation . . . 22
2.4.5 Correlator . . . 23
2.5 Calibration . . . 25
2.6 KVN geodetic VLBI measurement . . . 26

3 Observing proposal **27**

3.1 Observing mode . . . 27
3.1.1 Multi-frequency observation . . . 27
3.1.2 Fast position switching observation . . . 27
3.1.3 2 Gbps/4 Gbps/8 Gbps observation modes . . . 27
3.2 Angular resolution . . . 27
3.3 Baseline sensitivity . . . 28
3.4 System temperature . . . 28
3.5 Astrometric observation . . . 28

4 Observation and Data Reduction **28**
4.1 Preparation of observation and correlation 28
4.1.1 General information 28
4.1.2 Observation 30
4.1.3 Correlation 30
4.2 Data reduction 30
4.2.1 VLBI data reduction with AIPS 30
4.3 Correlator status 30
4.3.1 Daejeon Correlator 30
4.3.2 Software Correlator 30

5 Further information **31**

List of Tables

1 The geographical locations of the KVN antennas 7
2 Positions of KVN antennas in geocentric coordinates 8
3 Specifications for KVN antenna optics 8
4 Coefficients of normalized gain curves (the average of LCP and RCP) 9
5 Beam size, efficiencies, and DPFU[a] of each KVN antenna (the average of LCP and RCP 12
6 KVN Antenna Pointing Accuracy 14
7 AZ/EL beam offset with respect to the 86 GHz RCP beam 16
8 Frequency range of the KVN receiver 19
9 Noise temperature of the KVN receiver 20
10 System temperatures ($T_{\rm sys}$) using wide-band frequencies 20
11 KVN digital filter mode 21
12 KVN OCTAD mode 22
13 Available mode of the GPU spectrometer 23
14 Correlation mode of the KJCC 24
15 Angular resolutions at each KVN baseline and frequency 27
16 Baseline sensitivity of the KVN 28
17 Contact information 33

List of Figures

1 Korean VLBI Network (KVN) 5
2 The KVN antenna's design 6
3 UV coverage simulation for the K-band 7
4 Normalized gain curves of four bands (22, 43, 86, 129 GHz) at each KVN antenna 10
5 Aperture efficiencies and HPBWs of each KVN telescope. (a): Aperture efficiency, (b) HPBW 13
6 Beam patterns at Yonsei antenna. Top panels: Jupiter at 22 GHz (left) and 43 GHz (right), Bottom panels: Venus at 86 GHz (left) and 129 GHz (right). 14
7 The residual of pointing models at 43 GHz (KYS, KUS, KTN, from top to bottom) 15
8 Skylines of KYS, KUS, KTN, and KPC from top to bottom 17
9 KVN multi-frequency receiving system 18
10 KVN signal flows including a new wide-band sampler OCTAD (from 2020). . 19
11 System temperature changes with all wide-band frequencies 21
12 The trend of KVN antenna positions (IVP) in the ITRF 2014 coordinate system. The x and y axes are MJD and X, Y, and Z in meters. The linear fitting is applied to the measurements, shown as red line, and its deviation is also presented in each axis as "rms". 26
13 System temperatures of each KVN telescope 29
14 Data reduction flow chart with AIPS 31

15 A computing cluster and Lustre file system dedicated for the software correlation of the KVN. 32

1 Introduction

The Korean VLBI Network (KVN) is the only VLBI facility in Korea. It consists of four 21-m radio telescopes, located in Seoul (Yonsei University), Ulsan (University of Ulsan), Jeju Island, and Pyeongchang (newly constructed on the Pyeongchang campus of Seoul National University). This network has the same spatial resolution as a radio telescope with a range of 500-km (Figure 1). The KVN is, however, still small compared to American and European VLBI networks such as VLBA and EVN. To overcome this shortcoming, KASI has developed innovative multi-frequency band receiver systems that observe four different frequencies, i.e., K, Q, W, and D bands, simultaneously (center frequencies: 22, 43, 86, 129 GHz). With this capability, the KVN provides opportunities to study the formation and evolutionary processes of stars, the structure and dynamics of our galaxy, the nature of active galactic nuclei, and so on at milli-arcsecond resolution [1].

Figure 1: Korean VLBI Network (KVN)

2 KVN System

2.1 Network

2.1.1 Array

The Korean VLBI Network (KVN) is a four-element Very Long Baseline Interferometry (VLBI) network in Korea dedicated to VLBI observations at millimeter wavelengths. Four 21-m radio telescopes are situated in Seoul, Ulsan, Jeju, and Pyeongchang in South Korea; each is the KVN Yonsei Radio Telescope (hereafter KYS), the KVN Ulsan Radio Telescope (hereafter KUS), the KVN Tamna Radio Telescope (hereafter KTN), and the KVN Pyeongchang Radio Telescope (hereafter KPC), respectively. Baseline lengths range from 133 to 478 km. All antennas have the same design (Figure 2).

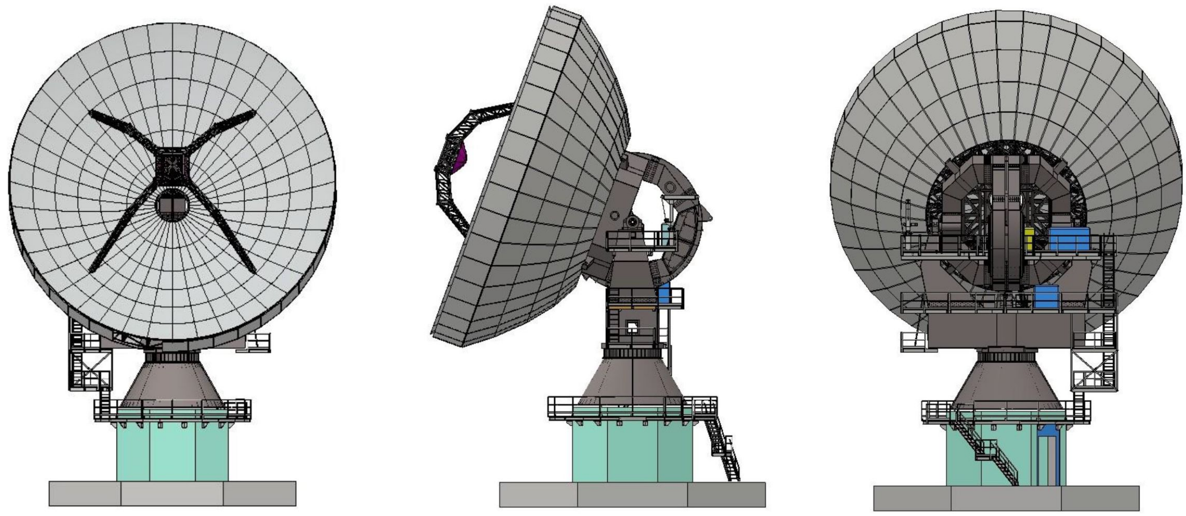

Figure 2: The KVN antenna's design

2.1.2 UV coverage

Figure 3 presents the simulated UV coverage of KVN at K-band for sources with varying declinations (+60, +30, 0, and -30 degrees) observed over 12 hours.

2.1.3 Antenna location

The coordinates of KVN antennas are shown in Table 1. Table 2 shows the locations of four KVN stations, sorted from north to south. All antenna locations are measured using GPS. KVN antenna positions are monitored regularly with GPS and geodetic VLBI observations in collaboration with VERA.

2.1.4 Array Operation Center (AOC)

KVN antennas can be remotely controlled by the Array Operation Center (AOC) at the East Asia VLBI Center, KASI, Daejeon. KVN stations are interconnected with the

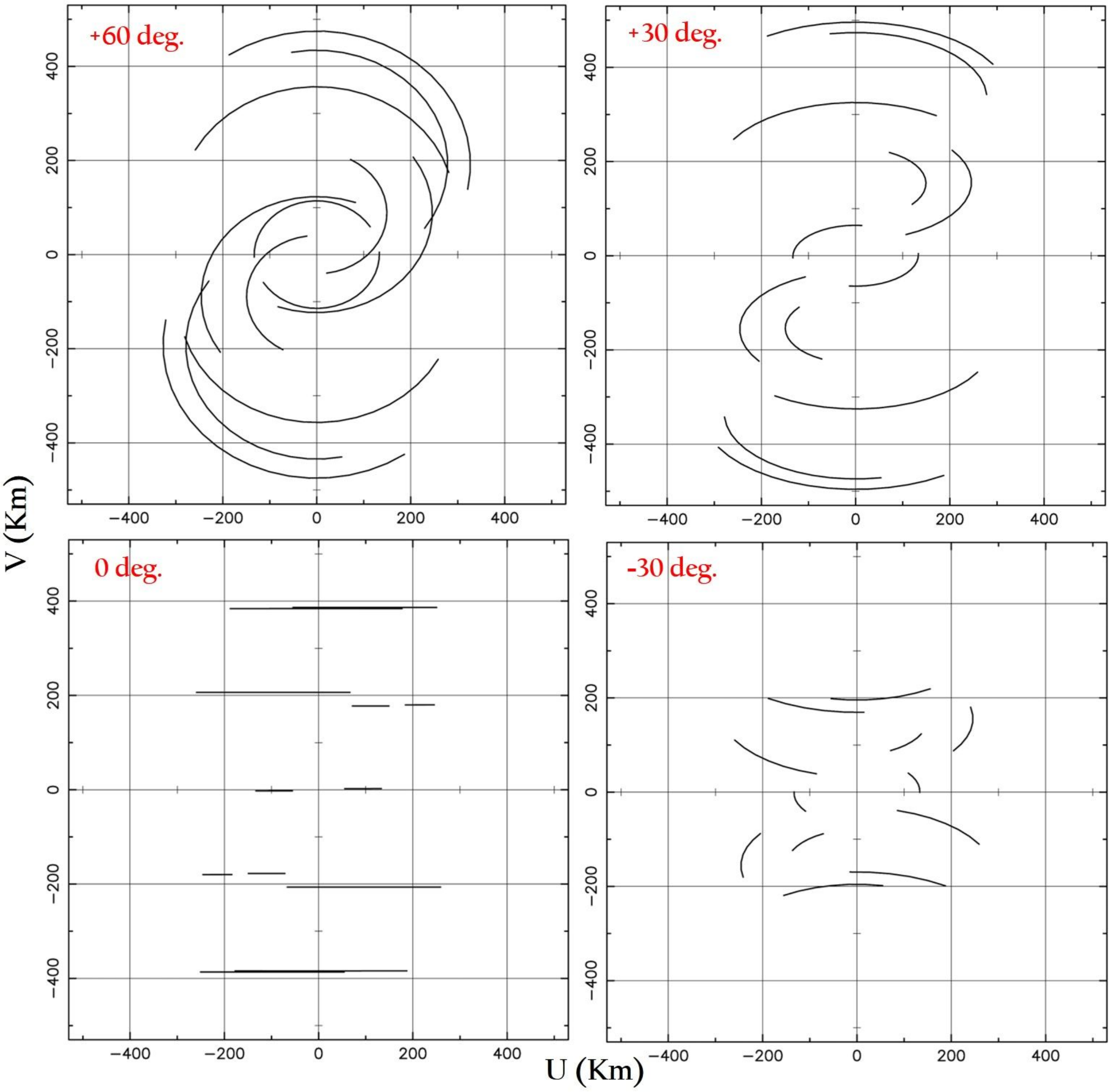

Figure 3: UV coverage simulation for the K-band

Table 1: The geographical locations of the KVN antennas

Antenna	Longitude (° ′ ″)	Latitude (° ′ ″)	Elevation (m)
KYS	126:56:27.4	37:33:54.9	139
KUS	129:14:59.3	35:32:44.2	170
KTN	126:27:34.4	33:17:20.9	452
KPC	128:26:55.1	37:32:00.1	541

AOC by a high-speed dedicated network called KREONET (Korea Research Environment Open NETwork). Considering the KVN antennas can be controlled remotely from the AOC,

Table 2: Positions of KVN antennas in geocentric coordinates

Antenna	MJD[a]	X (m)	Y (m)	Z (m)
KYS	58485	−3042281.0183	4045902.6730	3867374.3296
KUS	58485	−3287268.6453	4023450.1367	3687379.9886
KTN	58485	−3171731.6665	4292678.5393	3481038.7880
KPC	60033	−3149221.0525	3966404.9223	3864830.7006

[a] The coordinates is a Julian date.

it is vital that the AOC operator is aware of the weather conditions that can influence the quality of the VLBI data. Each KVN observatory has its own weather station that transmits information on air temperature, dew point, wind speed, wind direction, and air pressure to the AOC.

2.2 Antennas

2.2.1 Optics and Driving performance

The KVN antennas are shaped Cassegrain-type antennas with altitude-azimuth mounts. The main reflector of the telescope is 21 meters in diameter and has a focal length of 6.78 meters. The main reflector is made up of 200 aluminum panels with a manufacturing surface accuracy of approximately 65 μm. The main reflector's slewing speed is 3 °/second, allowing for fast position-switching observations. To compensate for the gravitational deformation of the main reflector and the sagging of the sub-reflector itself, the position, tilt, and tip of the sub-reflector are remotely controlled and modeled. The characteristics of the antenna optics are listed in Table 3.

Table 3: Specifications for KVN antenna optics

Main reflector (Axisymmetric Paraboloid)	Parameters
Diameter	D = 21.03 m
Focal length	f = 6.78 m
Focal ratio	f/D = 0.32
Panels manufacturing accuracy	65 μm
Alignment surface accuracy	50–54 μm
Sub-reflector (Hyperboloid) diameter	**Parameters**
Diameter	d = 2.25 m
Manufacturing surface accuracy	50 μm
Expected total surface accuracy	124 μm at EL 48°
Slewing speed	3 °/sec
Slewing acceleration	3 °/sec^2
Operating range	Az.: ±270°, El.: 0°–90°

2.2.2 Gain Curve

The main reflector panels of KVN antennas were installed to give the maximum gain at the elevation angle of $\sim 48°$. The sagging of the sub-reflector and the deformation of the main reflector by gravity with elevation results in degradation of antenna aperture efficiency with elevation. To compensate for this effect, a hexapod is utilized to adjust the sub-reflector position in KVN antennas. Although the hexapod correction reduces significantly the dependence of aperture efficiency with elevation, the degradation still appears evidently at a higher frequency. Figure 4 shows the elevation dependency of antenna gain of the KVN 21-m radio telescopes measured by observing several strong maser sources, Mars, and 3C 84, utilizing the observation mode of "Five pointing" or "Cross Scan".

We derived a normalized gain curve which has the following form: $G\_norm = A0{\cdot}EL^2 + A1{\cdot}EL + A2$, where EL is the elevation in degree, by fitting a second-order polynomial to the data and normalizing the fitted function with its maximum value. The fitted parameters are summarized in Table 4. The values displayed in Table 4 represent the average of LCP and RCP.

Table 4: Coefficients of normalized gain curves (the average of LCP and RCP)

Station	Frequency	A0	A1	A2
KYS	22	−8.9467E−06	5.4653E−04	9.9150E−01
	43	−2.4528E−05	1.4734E−03	9.7785E−01
	86	−5.6926E−05	4.7124E−03	9.0124E−01
	129	−1.5973E−04	1.3696E−02	7.0643E−01
KUS	22	−1.9115E−05	1.4894E−03	9.7040E−01
	43	−5.1311E−05	4.5593E−03	9.0199E−01
	86	−3.8227E−05	3.1453E−03	9.3526E−01
	129	−1.2589E−04	1.0413E−02	7.8466E−01
KTN	22	−1.0840E−05	9.6959E−04	9.7824E−01
	43	−1.6814E−05	1.7814E−03	9.5205E−01
	86	−5.6926E−05	4.7124E−03	9.0124E−01
	129	−1.1899E−04	1.2518E−02	7.4806E−01

2.2.3 Antenna beam size and Aperture efficiency

From December 2021 to March 2022, antenna panel adjustments were performed on three KVN telescopes (but not the KPC). As a consequence, the surface accuracy of three telescopes was enhanced to 70 (KYS), 72 (KUS), and 70 (KTN) μm, respectively. Furthermore, the KVN system was recently upgraded to a wide-band receiving system employing a new sampler, the OCTAD, encompassing the frequency ranges of 18–26 GHz (K), 35–50 GHz (Q), 85–116 GHz (W), and 125–142 GHz (D), respectively (see Section 2.3). Therefore, in all wide K, Q, W, and D bands, we measured HPBW, aperture efficiency, and main-beam efficiency using the OCTAD.

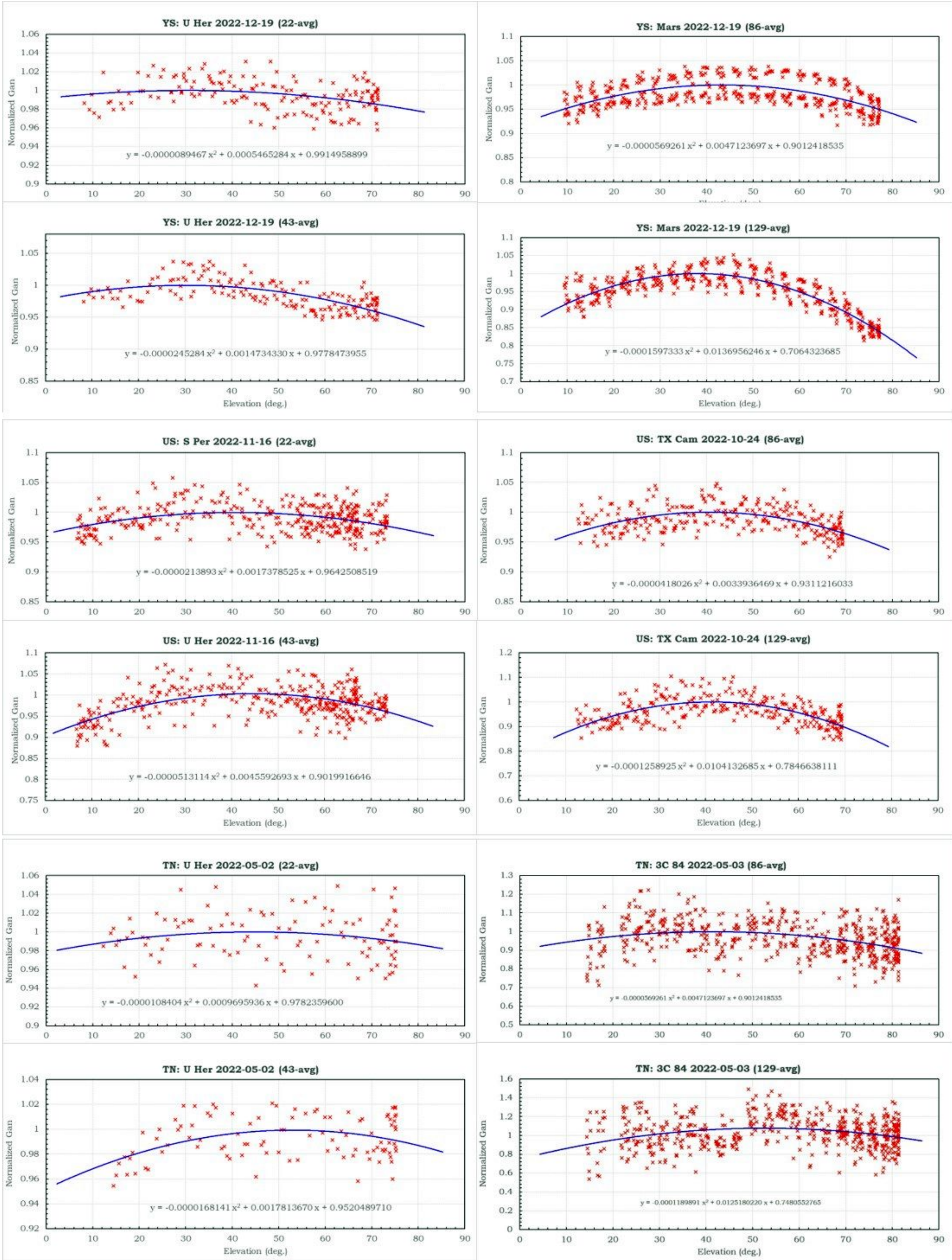

Figure 4: Normalized gain curves of four bands (22, 43, 86, 129 GHz) at each KVN antenna

The results of measurements of 22, 43, 86, and 129 GHz are shown in Table 5 as representative values for each band. While the W- and D-band values were acquired through observations toward Mars, the K- and Q-band values were obtained through observations toward Jupiter. The brightness temperatures for Jupiter in the K- and Q-bands are applied from de Pater et al. (2019)[2] and Maris et al. (2021)[3]. The estimates for the W- and D-bands use the Mars brightness modeling data that are displayed on its website[1]. Figure 5 displays the efficiency and beam size for each band of the telescopes.

- **Elevation dependency**
  With elevation, aperture efficiency changes. The previous section provided the gain curve that depicts the elevation dependency of the KVN antennas. The maximum values are those listed in Column (4).

- **Frequency dependency of beam efficiency**
  Beam efficiency also varies with beam size. The measured HPBWs are tabulated in Column (3), which are almost the same as the theoretical one (= λ/D of the antenna). To get a beam efficiency at 90 GHz, you have to multiply $(86/90)^2$ to that at 86 GHz.

- **Quantization correction of single-dish spectrum data**
  Prior to performing efficiency adaptations, single-dish spectrum data must be multiplied by a factor of 1.25 if it is being reduced. This is to compensate for the effects of the digital filter and spectrometer.

- Parameters of Table 5 can be applied for the following observing season;
  - KYS: from February 2023 – now
  - KUS: from February 2023 – now
  - KTN: from March 2023 – now

2.2.4 Beam pattern

The optics of the KVN antenna are of the shaped-Cassegrain type, in which the main reflector and sub-reflector are shaped to have a uniform illumination pattern on an aperture plane. KVN antennas are able to provide more aperture efficiency than conventional Cassegrain-type antennas because of the uniform illumination. A higher sidelobe level is unavoidable, though. Figure 6 shows OTF images of Venus and Jupiter at 86 and 129 GHz and 22 and 43 GHz, respectively, as measured using the Yonsei antenna. For 22 and 43 GHz, the map is $12' \times 10'$ in size, and for 86 and 129 GHz, the size is $3.5' \times 3'$. One can see the first sidelobe pattern. KVN antennas typically have sidelobe levels of $-(14{\sim}13)$ dB.

2.2.5 Antenna pointing accuracy

Since 2009, a sample of late-type evolved stars has been utilized to determine the telescope's pointing accuracy. We show the accuracy of the pointing models for three KVN radio telescopes that were set up in May and November 2022 in Table 6. For each epoch and

[1] `https://lesia.obspm.fr/perso/emmanuel-lellouch/mars/`

Table 5: Beam size, efficiencies, and DPFU[a] of each KVN antenna (the average of LCP and RCP

Site	Frequency (Band) (GHz)	HPBW (arcsec)	η_A (%)	η_B (%)	DPFU (K/Jy)
(1)	(2)	(3)	(4)	(5)	(6)
KYS	22 (K)	133	67	58	0.0840
	40 (Q-low)	73	70	60	0.0876
	43 (Q-high)	67	72	62	0.0908
	47 (Q-high)	64	71	60	0.0887
	86 (W-low)	32	53	41	0.0661
	95 (W-low)	30	46	38	0.0572
	103 (W-high)	28	46	39	0.0582
	111 (W-high)	27	46	40	0.0572
	129 (D)	25	36	34	0.0452
	140 (D)	24	31	35	0.0387
KUS	22 (K)	131	78	65	0.0978
	40 (Q-low)	72	68	58	0.0855
	43 (Q-high)	66	73	61	0.0921
	47 (Q-high)	61	66	57	0.0833
	86 (W-low)	32	63	48	0.0790
	95 (W-low)	29	58	45	0.0723
	103 (W-high)	27	56	45	0.0698
	111 (W-high)	26	55	47	0.0685
	129 (D)	23	44	40	0.0554
	140 (D)	21	42	38	0.0521
KTN	22 (K)	131	67	58	0.0840
	40 (Q-low)	69	59	47	0.0745
	43 (Q-high)	68	63	55	0.0795
	47 (Q-high)	59	56	45	0.0705
	86 (W-low)	32	57	46	0.0720
	95 (W-low)	29	53	43	0.0666
	103 (W-high)	28	51	43	0.0645
	111 (W-high)	27	44	40	0.0548
	129 (D)	23	38	34	0.0474
	140 (D)	22	33	32	0.0417

[a] indicates the Degree Per Flux density Unit.
η_A: Aperture efficiency.
η_B: Main-beam efficiency.

telescope, the total, azimuth, and elevation of the root mean square (rms) of the residual pointing offsets between the observations and the pointing models are reported, accordingly ($Total\,Error = Sqrt(Az\_Error^2 + El\_Error^2)$). Figure7 displays the residual of each KVN telescope's pointing model.

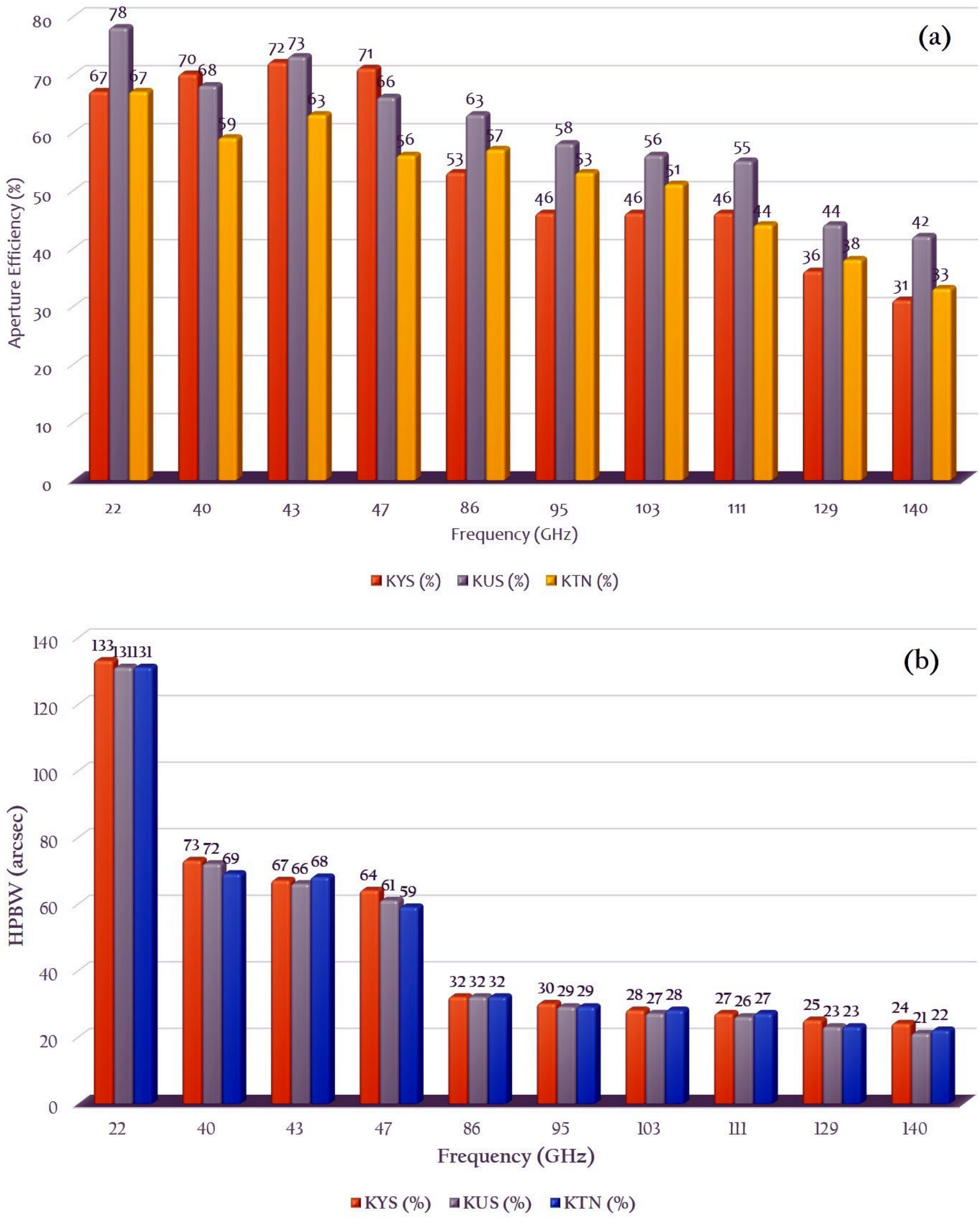

Figure 5: Aperture efficiencies and HPBWs of each KVN telescope. (a): Aperture efficiency, (b) HPBW

It is necessary to make pointing observations at least every hour during the day, especially at sunrise and sunset, in order to keep the pointing accuracy at fewer than 6 arcseconds in the root mean square.

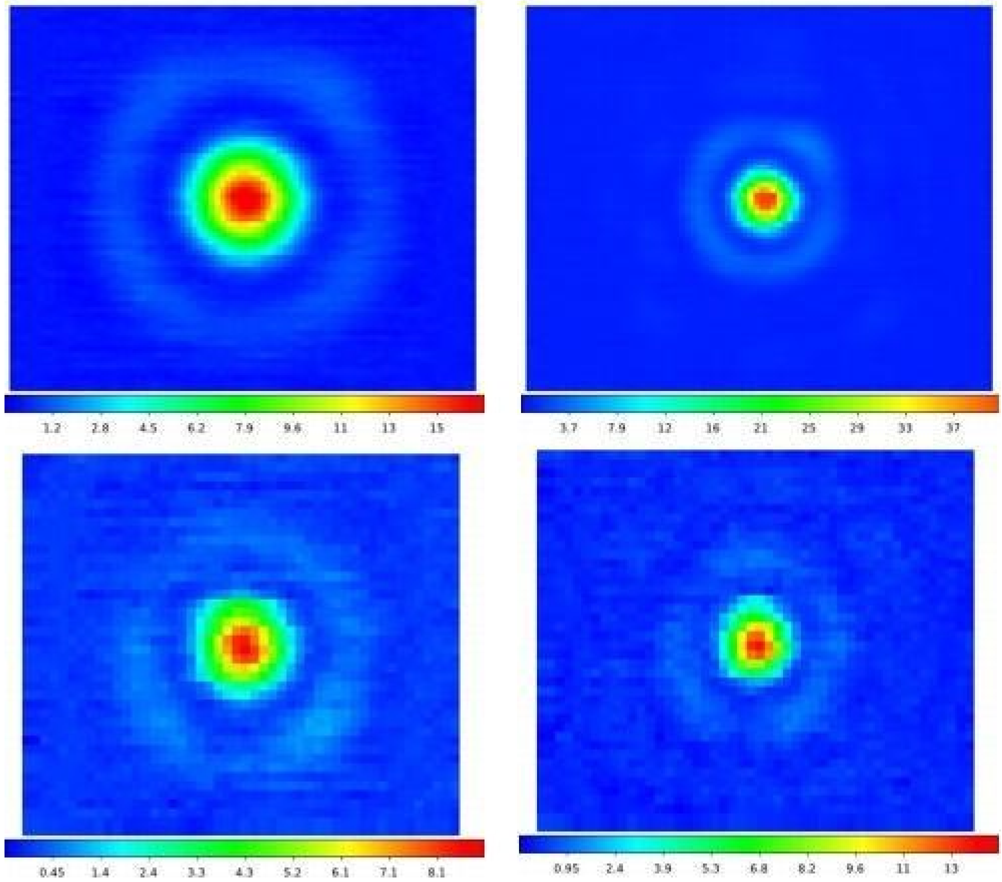

Figure 6: Beam patterns at Yonsei antenna. Top panels: Jupiter at 22 GHz (left) and 43 GHz (right), Bottom panels: Venus at 86 GHz (left) and 129 GHz (right).

Table 6: KVN Antenna Pointing Accuracy

Site	Total (arcsec)	Azimuth (arcsec)	Elevation (arcsec)	Frequency (GHz)	Date
KYS	5.84	4.06	4.20	43	Nov. 20 2022
KUS	5.32	2.75	4.55	43	May 24 2022
KTN	3.96	2.06	3.38	43	Nov. 21 2022

2.2.6 Beam alignment

The quasi-optics should be set up for simultaneous observations of the four frequency bands such that each of the four beams is directed towards the same point in the sky. The other frequency bands' pointing offsets from the 86 GHz RCP beam's center are summarized in Table 7. After alignment, the cross-scan results were used to calculate the relative offsets. As a consequence, the 129 and 43 GHz beams are aligned within 3 arcseconds, whereas the beam at 22 GHz is aligned within 5 arcseconds.

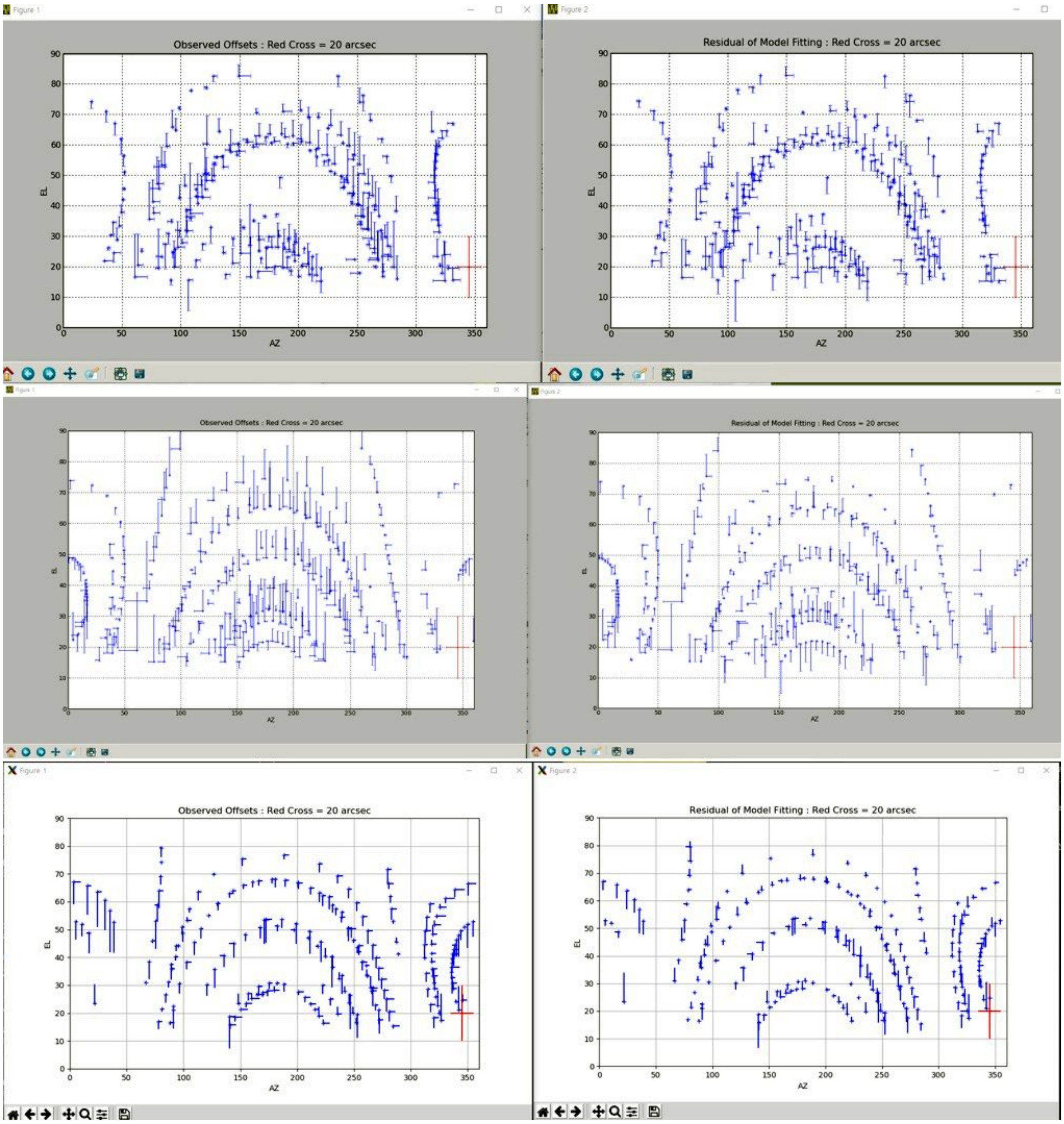

Figure 7: The residual of pointing models at 43 GHz (KYS, KUS, KTN, from top to bottom)

2.2.7 Skylines

Skylines are the limits of the viewable height with azimuth below which we cannot see the sky. These limits are determined by obstructions caused by the neighboring buildings, trees, and mountains. Skylines of KVN sites measured in 2014 are shown in Figure 8. In addition, the skyline of the recently constructed KVN Pyeongchang Radio Telescope (KPC) was measured in August 2019.

Table 7: AZ/EL beam offset with respect to the 86 GHz RCP beam

Site	Band (L, R) (GHz)	Az. offset (arcsec)	El. offset (arcsec)	Date
KYS	22 (L)	−0.8 (±0.4)	−0.4 (±0.4)	Dec. 19 2022
	22 (R)	−1.7 (±0.4)	−0.9 (±0.4)	Dec. 19 2022
	43 (L)	+1.1 (±0.3)	−0.9 (±0.2)	Dec. 19 2022
	43 (R)	+0.4 (±0.4)	−1.3 (±0.3)	Dec. 19 2022
	86 (L)	−2.3 (±0.0)	0.0 (±0.0)	Dec. 19 2022
	86 (R)			Dec. 19 2022
	129 (L)	+0.7 (±0.7)	−0.9 (±0.2)	Dec. 19 2022
	129 (R)	−0.7 (±0.7)	−0.6 (±0.2)	Dec. 19 2022
KUS	22 (L)	−0.8 (±0.5)	+2.0 (±0.6)	Sep. 30 2021
	22 (R)	−1.6 (±1.4)	+3.1 (±0.1)	Sep. 30 2021
	43 (L)	−0.5 (±0.2)	+0.4 (±0.1)	Sep. 30 2021
	43 (R)	−1.0 (±0.0)	+0.3 (±0.0)	Sep. 30 2021
	86 (L)	−1.4 (±0.1)	−0.1 (±0.1)	Sep. 30 2021
	86 (R)			Sep. 30 2021
	129 (L)	−1.0 (±0.2)	+1.5 (±0.3)	Sep. 30 2021
	129 (R)	−1.3 (±0.1)	+1.1 (±0.4)	Sep. 30 2021
KTN	22 (L)	−2.6	+0.8	
	22 (R)	−3.6	−0.1	
	43 (L)	+0.3	−2.5	
	43 (R)	+0.1	−1.8	
	86 (L)			
	86 (R)	+2.1	0.0	
	129 (L)	+2.0	−1.2	
	129 (R)	+0.8	−1.4	

2.3 Receiver

2.3.1 Quasi-optics

The KVN has the unique capability to observe four frequency bands [4], simultaneously. KVN quasi-optics are designed to enable this multi-frequency observation. Figure 9 shows the layout of quasi-optics and receivers viewing from the sub-reflector side. The quasi-optics system splits one signal from the sub-reflector into four using three dichroic low-pass filters marked as LPF1, LPF2, and LPF3 in the figure. The split signals into four different frequency bands are guided to corresponding receivers.

2.3.2 Block diagram

The 22 (K), 43 (Q), and 86 (W) GHz band receivers are cooled HEMT receivers, and the 129 (D) GHz band receiver is an SIS mixer receiver [5]. All receivers receive dual-circular-polarization signals. Among eight signals (four dual-polarization signals), four signals se-

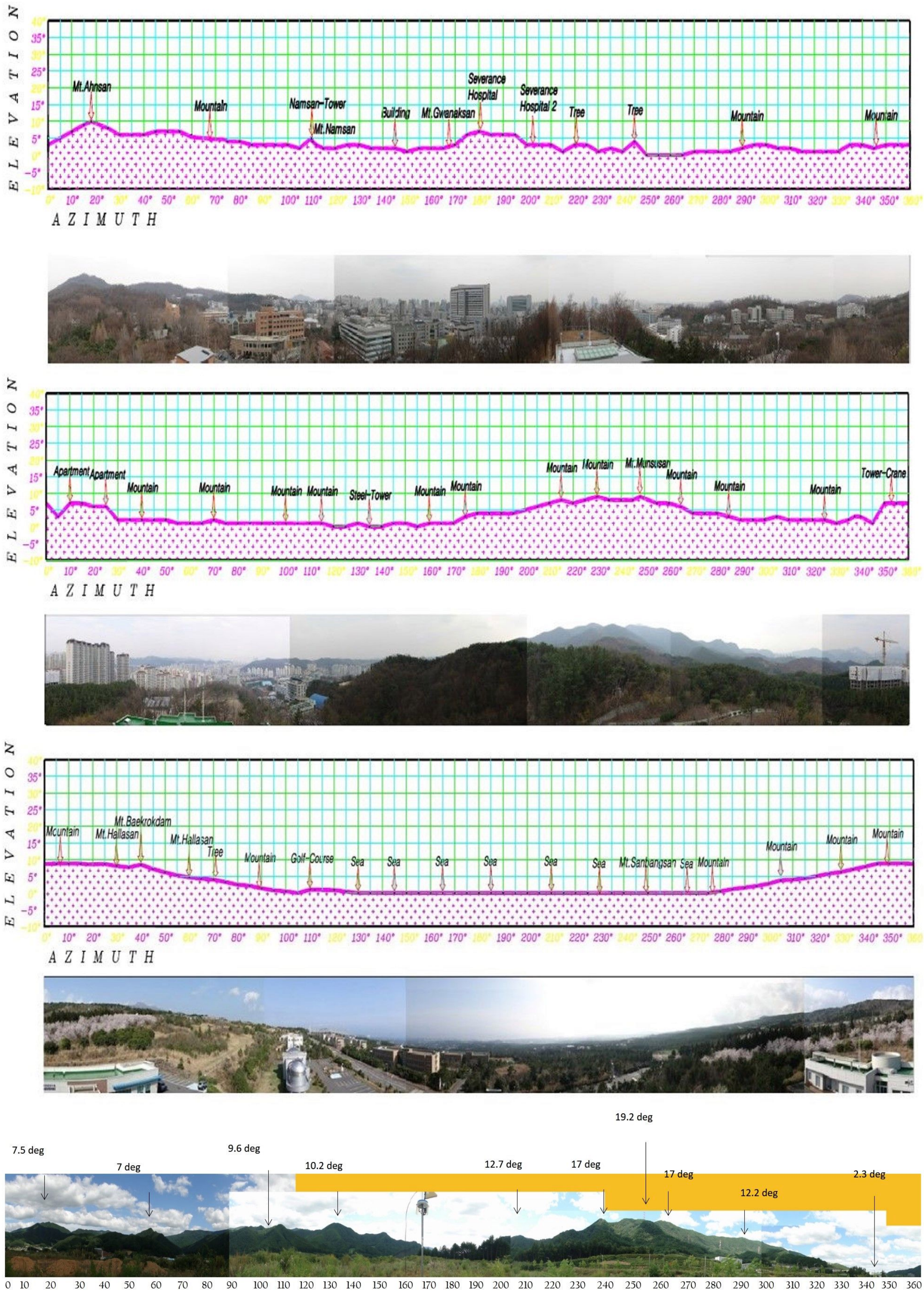

Figure 8: Skylines of KYS, KUS, KTN, and KPC from top to bottom

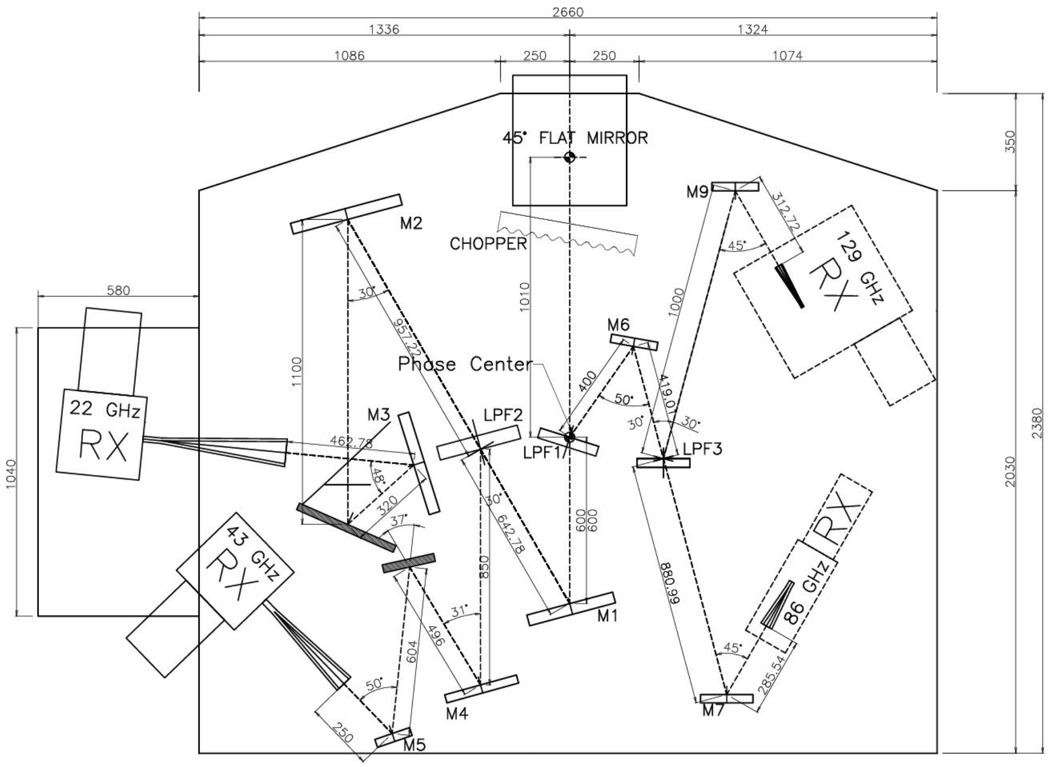

Figure 9: KVN multi-frequency receiving system

lected by the IF selector are down-converted to the input frequency band of the sampler. The samplers digitize signals into 2-bit data streams with four quantization levels. The sampling rate is 1024 Mega samples per second, resulting in a 2 Gbps data rate (2-bit $\times$ 1024 megabytes per second) and 512 MHz frequency bandwidth. In total, we can get 4 streams of 512 MHz bandwidth (2 Gbps data rate) simultaneously, which means that the total rate is 8 Gbps.

New wide-band VLBI backends, including OCTAD, Mark 6, and GPU spectrometers, are introduced for wide-band operation. They are indicated in the red box of Figure 10. The OCTAD consists of four analog-to-digital converters, digital signal processing modules, and a VDIF formatter. It digitizes four IF signals and performs signal processing for digital down-conversion and filtering. Combining OCTAD and ADS1K+Fila10G, all eight IF signals (four dual-polarization signals) can be obtained at the same time. The OCTAD has four 10 GbE outputs, with which we can get a maximum 32 Gbps aggregated data rate.

2.3.3 Frequency range

The instantaneous bandwidth of the 1st IF of each receiver is limited to 8 GHz by the band-pass filter. Table 8 shows the frequency range of each receiver. The Q- and W-bands are divided into two frequency ranges. The low (high) frequency ranges of the Q-band receiver are from 35 (42) to 42 (50) GHz. The low (high) frequency ranges of the W-band receiver are from 85 (100) to 100 (116) GHz. Low- and high-frequency bands of the same polarization cannot be observed at the same time. Note that the D-band receiver has 2 GHz

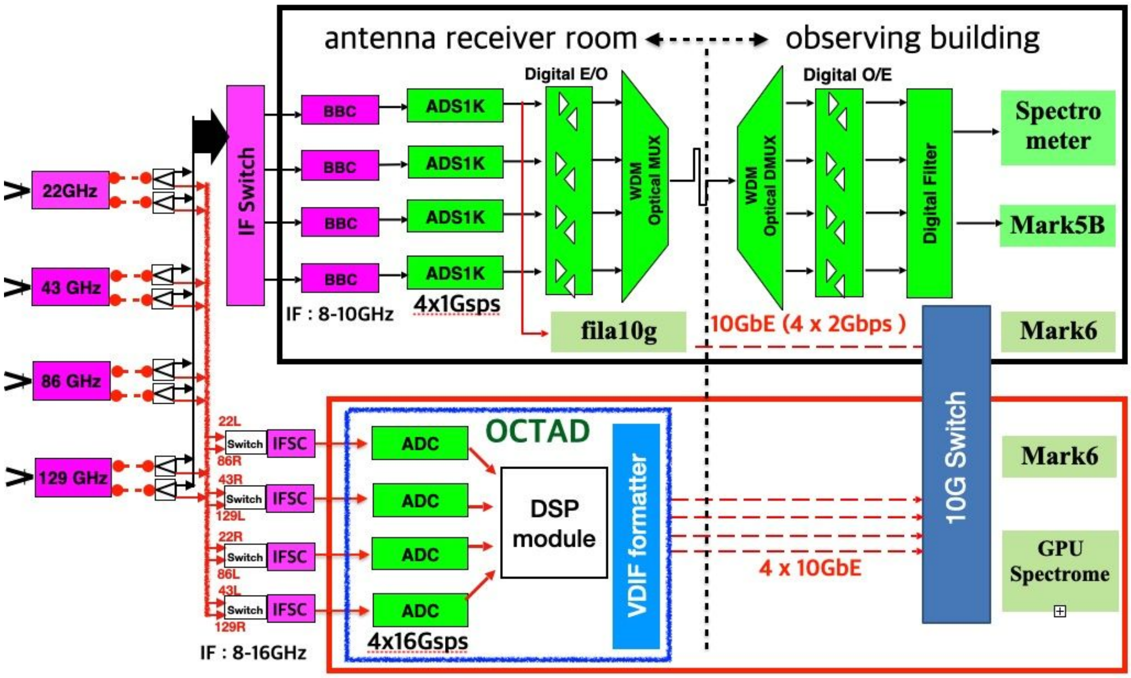

Figure 10: KVN signal flows including a new wide-band sampler OCTAD (from 2020).

IF bandwidth.

Table 8: Frequency range of the KVN receiver

Band	Frequency range (GHz)	IF range (GHz)
K	18.0 – 26.0	8.192 – 16.384
Q	35.8 – 42.0 (Low)	8.192 – 16.384
	42.1 – 50.0 (High)	
W	85.0 – 100.0 (Low)	8.192 – 16.384
	100.1 – 115.8 (High)	
D	125.0 – 142.0	8.0 – 10.0

2.3.4 Receiver noise temperature

The typical noise temperature for each band is displayed in Table 9. The loss of quasi-optics does not reduce the efficiency of the antenna aperture since the calibration chopper is placed before the quasi-optics; rather, it raises the temperature of the receiver noise. As a result, 40-–50 K are added to the noise temperatures to account for the quasi-optics losses.

2.3.5 System temperatures with wide-band frequencies

Wide-band observations are now possible with the KVN thanks to the integration of the GPU spectrometer and a new backend (OCTAD). In this regard, we evaluated the system

Table 9: Noise temperature of the KVN receiver

Bnad	$T_{\rm rx}$ (K)
K	50 – 80
Q	50 – 80
W	50 – 80
D	50 – 80

temperatures over all wide-band frequency ranges, and the results are presented in Table 10 and Figure 11.

Table 10: System temperatures ($T_{\rm sys}$) using wide-band frequencies

Site	Band	Freq. range (GHz)	$T_{\rm sys}$ (K)	El. (degree)	Date
KYS	K	18.0 – 26.0	82 – 98	45 – 49	Jan. 17 2023
	Q-low	35.8 – 42.0	60 – 112	51 – 52	Jan. 17 2023
	Q-high	42.1 – 50.0	91 – 140	45 – 48	Jan. 17 2023
	W-low	85.0 – 100.0	147 – 191	59 – 65	Jan. 27 2023
	W-high	100.1 – 115.8	131 – 255	40 – 43	Feb. 01 2023
	D	125.0 – 142.0	139 – 180	35 – 51	Jan. 27 2023
KUS	K	18.0 – 26.0	71 – 91	55 – 56	Feb. 08 2023
	Q-low	35.8 – 42.0	51 – 118	51 – 52	Feb. 08 2023
	Q-high	42.1 – 50.0	85 – 156	46 – 48	Feb. 08 2023
	W-low	85.0 – 100.0	153 – 203	48 – 61	Feb. 08 2023
	W-high	100.1 – 115.8	150 – 315	43 – 61	Feb. 10 2023
	D	125.0 – 142.0	145 – 279	36 – 46	Feb. 08 2023
KTN	K	18.0 – 26.0	71 – 77	59 – 62	Feb. 20 2023
	Q-low	35.8 – 42.0	58 – 85	49 – 58	Feb. 20 2023
	Q-high	42.1 – 50.0	79 – 121	58 – 59	Feb. 20 2023
	W-low	85.0 – 100.0	114 – 159	59 – 65	Feb. 20 2023
	W-high	100.1 – 115.8	101 – 142	57 – 63	Feb. 21 2023
	D	125.0 – 142.0	121 – 163	37 – 48	Feb. 24 2023

2.4 Digital Process

2.4.1 Digital filter mode

The digital filter bank (DFB) is configurable to various modes according to the required number of streams and bandwidths. The DFB enables us to select in frequency domain 16 data streams of 16 MHz bandwidth from 4 streams of 512 MHz bandwidth. The corresponding data rate of the 16×16 MHz stream is 1024 Mbps, which corresponds to the maximum input data rate of the Mark5b recorder. Combining more than one stream, the DFB can

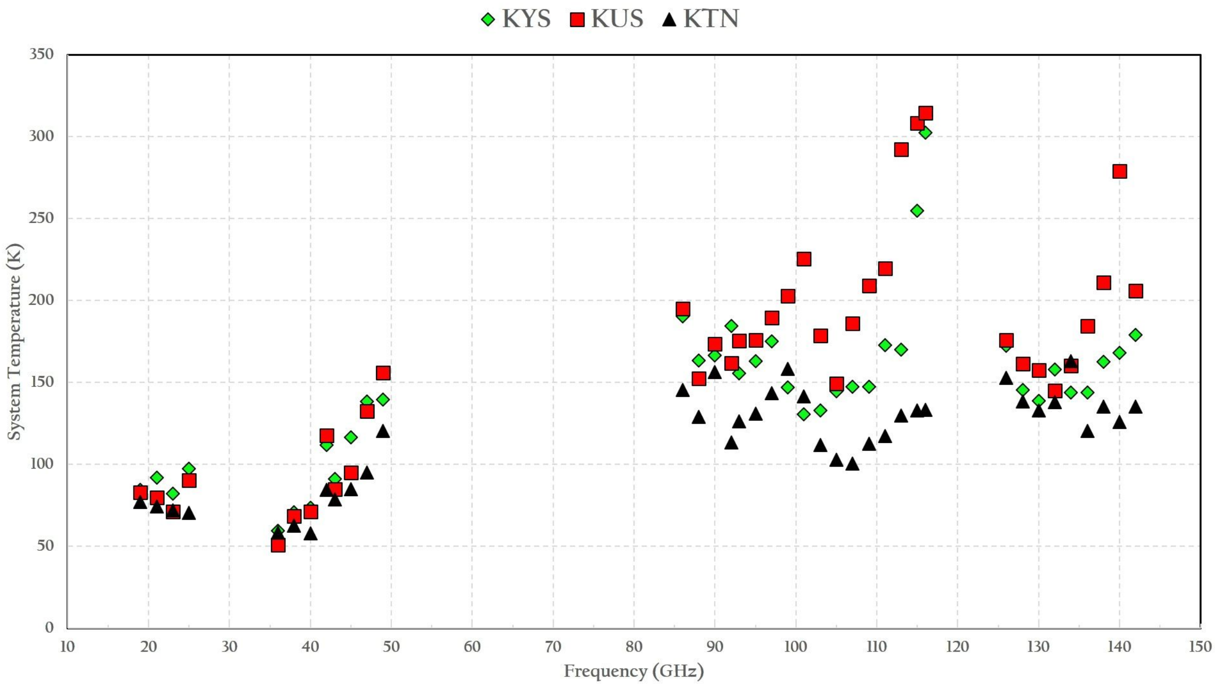

Figure 11: System temperature changes with all wide-band frequencies

produce streams with wider bandwidth such as 8×32 MHz, 4×64 MHz, 2×128 MHz, and 1×256 MHz (see Table 11).

Table 11: KVN digital filter mode

Bandwidth (MHz)	Number of streams
16	16
32	8
64	4
128	2
256	1

A center frequency of a data stream is given by $\mathrm{BW} \cdot (0.5 + \mathrm{N})$, where BW and N represent a bandwidth of data stream and integer number, respectively. If N is an even number, the data stream is the upper sideband. Otherwise, the data stream is in the lower sideband. Therefore, adjacent data streams have opposite sidebands. The center frequency cannot exceed 512 MHz.

2.4.2 Signal processing mode of OCTAD

The OCTAD provides various configurable modes. It enables us to select in the frequency domain a maximum of 16 data streams from 4 streams of 8192 MHz bandwidth. The maximum output rate is 32 Gbps (4×8 Gbps) of which the net bandwidth is 8 GHz (4×2 GHz

Table 12: KVN OCTAD mode

Bandwidth (MHz)	Max. Number of streams	Total data rate (Gbps)
16	16	1
32	16	2
64	16	4
128	16	8
256	16	16
512	16	32
1024	8	32
2048	4	32

bandwidth). The possible mode of OCTAD is listed in Table 12. There is no restriction on the frequency step and the order of sideband in the OCTAD digital down-converter, unlike the digital filter.

2.4.3 Recorders

KVN station has two recording systems, Mark5b and Mark6.

Mark5b and Mark6 are hard disk recording systems developed at Haystack Observatory, USA. The maximum data rate of Mark5b and Mark6 systems is 1 Gbps and 16 Gbps, respectively. For more details, please see `https://www.haystack.mit.edu/haystack-memo-series/mark-5-memos/` and `https://www.haystack.mit.edu/haystack-memo-series/mark-6-memos/`. At KVN stations, the Mark5b records the output data stream of a digital filter. Refer to section 2.3.2 for data stream connection and section 2.4.1 for available bandwidth and number of channels of 1 Gbps data stream.

Mark6 records output data streams of four samplers via Fila10G. The Fila10G converts four VSI streams from four samplers into VDIF (VLBI Data Interchange Format) data and sends them to the Mark6 on a 10 GbE network connection. There is no digital filtering function in the Fila10G. Therefore, single IF of Mark6 data of the KVN always has 512 MHz bandwidth. 2 Gbps (1 IF $\times$ 512 MHz), 4 Gbps (2 IF $\times$ 512 MHz) and 8 Gbps (4 IF $\times$ 512 MHz) modes are available in the KVN using the Mark6. The OCTAD VDIF output can be recorded by Mark6. For OCTAD 32 Gbps mode, all two Mark6 should be employed only for the OCTAD output. We cannot record Fila10G output. Therefore, we can observe no more than four IF signals among eight in OCTAD 32 Gbps mode.

2.4.4 Spectrometers for Single-dish observation

- **Digital spectrometer**
  The VSI output data from the digital filter with an aggregation rate of 1024 MHz (256 MHz bandwidth) is processed using an FX-type digital spectrometer (DSM). The DSM is capable of processing 4 VSI streams that are sent from samplers via optical transmission. It processes data with a bandwidth of 4×512 MHz. It is capable of generating both cross- and auto-power spectrum data. For the purpose of observing

Table 13: Available mode of the GPU spectrometer

Bandwidth (MHz)	Number of streams	Total data rate (Gbps)
32	16	2
64	16	4
128	16	8
256	8	8
512	4	8
1024	2	8
2048	1	8

polarization, cross-power spectrum measurements are employed. In all modes, the total number of FFT points accessible is set at 4096 channels per stream.

- **GPU Spectrometer**
  The GPU (Graphics Processing Unit) spectrometer processes VDIF data streams from OCTAD to create a power spectrum using FFT computations. The modalities that are accessible vary depending on the performance of the GPU cards and the host server of the GPU spectrometer in each station. Table 13 provides a summary of them. Because of its considerable flexibility, the GPU spectrometer can accommodate various numbers of FFT points. In a 32 MHz stream, we can obtain at least 4096 FFT points. As with a digital spectrometer, the GPU spectrometer can generate both auto- and cross-power spectrum data. However, because it is still under testing and evaluation, the polarization observation mode employing the GPU spectrometer's cross-power spectrum output is not currently available.

2.4.5 Correlator

- **Correlators in KJCC**
  KJCC(Korea-Japan Correlation Center) gathers the raw VLBI observation data from each site of KVN, VERA/JVN, and CVN, and performs the correlation process with two VLBI correlators.

  The first one, Daejeon Correlator, is one of the fastest VLBI correlators in the world and is used for processing the KaVA and EAVN observations mainly. It is capable to correlate the data streams of max. 8 Gbps for max. 16 stations in one pass, to produce the correlated output of 8192 spectral points for each sub-bands. The number of spectral points is reduced to 128 for continuum, 512 for line observation after the correlation process by channel integration.

  The second one, DiFX (Distributed FX), is the world-famous software correlator and is used for processing the KVN observations. It provides quite flexible correlation modes. You can request the accumulation time and the frequency resolution appropriate for your science purpose.

For the final correlation output, the default accumulation time is 1.6384 seconds for the Daejeon correlator or 0.8192 seconds for DiFX correlator. The final frequency resolutions are 16 MHz/128 for continuum observations, and 16 MHz/512 for line observations in default.

- **Correlation mode and integration time**
  The KJCC is currently able to support the following correlation modes (see Table 14).

Table 14: Correlation mode of the KJCC

Obs. Mode	Total Data Rate	Bandwidth /sub-band	# of sub-bands	Minimum Accum. Time	# of Freq. Channels /sub-band
C5	1024 Mbps	16 MHz	16	1.6384 sec	8192
C4	1024 Mbps	32 MHz	8	0.8192 sec	8192
C3	1024 Mbps	64 MHz	4	0.4096 sec	8192
C2	1024 Mbps	128 MHz	2	0.2048 sec	8192
C1	1024 Mbps	256 MHz	1	0.1024 sec	8192
W1	2048 Mbps	512 MHz	1	0.0512 sec	8192
W2	4096 Mbps	512 MHz	2	0.0512 sec	8192
W4	8192 Mbps	512 MHz	4	0.0512 sec	8192

- **CODA and FITS**
  The KJCC supports the following number of frequency channels for preparing FITS file.
  - Basic output channel of correlator: 8192 frequency channel
  - Continuum: 128 frequency channel (64 channels integrated in post-correlation)
  - Spectral line: 512 frequency channel (16 channels integrated in post-correlation)
- **FITS delivery**
  Correlations will be done using either the DiFX or the Daejeon correlator. The KJCC will deliver the FITS file to PI by using an FTP server or mobile disk.
  - When correlation is finished, the FITS file will be prepared through post-processing, and then the KJCC will announce the correlation processing completion to the PI by email. In the email, PI will be able to get the FITS file via a temporary URL link.
  - The PI should download the FITS file as soon as possible and check the FITS file using his or her preferred analysis tool. And then the PI should give his response to KJCC with "Success" (data quality is good) or "Fail" (download fail, bad FITS file, data quality is bad, etc.). Especially in the case of the "Fail" opinion, please send the error message to the KJCC, Your quick response for the FITS will be helpful for the KJCC to solve the problem as soon as possible.
  - The KJCC would like to receive PI's response within 2 weeks after announcing the email. If there is no response within 4 weeks, the KJCC determines that the PI's response is regarded as "success".

  - In case of "Fail", according to the fail type, the KJCC will conduct the URL check, file reconstruction, or re-correlation, and then an announcement will be sent again to PI via e-mail.
  - In the case of "Success", correlation processing for that observation will be closed (at that time, the download link in the temporary URL will be unavailable), and the tapes or disk modules will be included in the release pool for recycling.
  - The FITS file provided to PI will be stored separately at the observation data archive. The PI should analyze, perform the research, and publish the paper within some period of time (in general, 18 months). After 18 months, the FITS file stored in the archive system will be opened to the public, who will need to do their research using that FITS according to the procedures.

- **Archiving policy**
  The KJCC organizes the archiving policy for observation data, CODA, and FITS files as below.
  - Observation data: 2 weeks after FITS release (usually, about 2 months after observation), and then it will be released.
  - CODA: If correlated data is used for astrometry or geodesy, it is permanently stored at the CODA server. Otherwise, the correlated raw data and CODA file system will be deleted after receiving the response from PI.
  - FITS: it is permanently archived at the Archiving server.

- **Expected time of correlation**
  Correlation processing will take about 1 week to prepare the first version of FITS after the data arrives from the last station. However, the KJCC team will do their best to make correlation results available as quickly as possible to deliver the FITS file to PI.

2.5 Calibration

System temperatures in Kelvin ($T_{\rm sys}$) are measured during observations at KVN stations once every user-specified interval (default 10 sec) to calibrate amplitude variation in time due mainly to atmospheric fluctuation. The measured $T_{\rm sys}$ is a sum of three temperatures: the receiver temperature, the spillover temperature, and the contribution of the atmosphere as described in Petrov et al. (2012) [6]. These $T_{\rm sys}$ values can be converted to SEFD (System Equivalent Flux Density) by dividing by the KVN antenna gains in K/Jy. The elevation dependence of the antenna gains is also corrected based on the normalized gain curves with lease-squared-fitted second-order polynomials as derived in Lee et al. (2011) [7].

Additional amplitude correction for the atmospheric opacity above an antenna is performed by conducting a sky tipping curve analysis according to the method described in Mangum (2000). In practice, the system temperatures ($T^*_{\rm sys}$) corrected for the atmospheric opacity are estimated based on the sky tipping curve measurements once every user-specified interval (default before and after an experiment). Further corrections are made to the KVN observations taken with 2-bit (4-level) sampling, for the systematic effects of the non-optimal setting of the quantizer voltage thresholds.

The amplitude calibrations with the KVN are accurate to 15 % or better at 22 and 43 GHz. However, it is recommended to observe a few amplitude calibrators during the scheduled observation time, allowing for (a) the assessment of the relative gains of KVN antennas and gain differences between IF-bands at each station, and (b) the confirmation of the correlation coefficient correction assuming that you have contemporaneous source flux densities obtained with other VLBI networks independent of the KVN observations.

2.6 KVN geodetic VLBI measurement

Obtaining accurate antenna positions is important in the VLBI system, especially for high precision astrometry. KVN antenna positions are regularly monitored using GPS and geodetic VLBI observations. The K-band geodesy VLBI program between KVN and VERA started in 2011. Current KVN antenna positions (see Figure 12) were obtained from the KaVA K-band geodesy on January 24, 2014. The typical 1-sigma errors of geodetic solutions are about 0.4 cm in the X, Y, and Z directions. Based on 22-epoch KaVA K-band geodetic observations from September 2012 to December 2016, uncertainties of KVN antenna positions are $\sim$ 2.38 cm at KYS, $\sim$ 2.55 cm at KUS, and $\sim$ 1.58 cm at KTN.

The KVN antenna positions are described in Section 2.1.3.

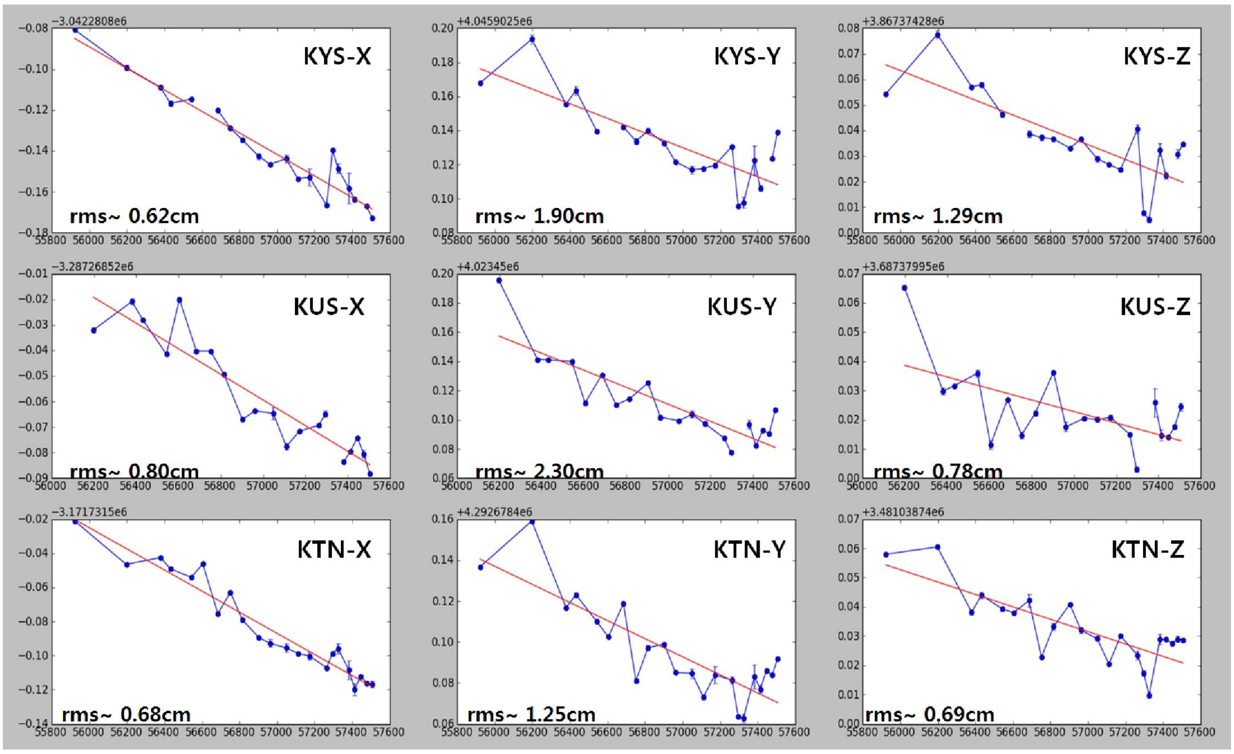

Figure 12: The trend of KVN antenna positions (IVP) in the ITRF 2014 coordinate system. The x and y axes are MJD and X, Y, and Z in meters. The linear fitting is applied to the measurements, shown as red line, and its deviation is also presented in each axis as "rms".

3 Observing proposal

3.1 Observing mode

3.1.1 Multi-frequency observation

Simultaneous multi-frequency observation is a unique capability of the KVN, with which we can calibrate out the short-term phase fluctuations at higher frequency data by referencing the phase solution obtained from lower frequency data. This phase referencing technique allows us to integrate the data for a time scale much longer than the coherent time scale of atmospheric phase fluctuation and so to observe weak sources at mm-wavelength efficiently. For multi-frequency observations, we can select no more than 4 IFs among 8 IF signals (= 4 receivers $\times$ 2 polarizations).

3.1.2 Fast position switching observation

The slewing speed and acceleration rate of the KVN antenna are 3 $^{\circ}$/sec and 3 $^{\circ}$/sec^2, respectively. Due to this high speed and acceleration rate, the KVN antenna can switch its pointing from target to calibrator in a short period of time.

3.1.3 2 Gbps/4 Gbps/8 Gbps observation modes

2 Gbps (1×512 MHz), 4 Gbps (2×512 MHz), 8 Gbps (4×512 MHz) modes, which use fila10G and Mark6 recorders, have been fully evaluated in 2017. These modes are available for common use observations from the 2017B semester. For multi-frequency observations, we can select 1, 2, or 4 IFs among 8 IF signals (= 4 receivers $\times$ 2 polarizations). Note that it is not allowed to assign multiple 512 MHz streams to one IF.

3.2 Angular resolution

Table 15 shows the maximum lengths (B) of the KVN baselines in km and the corresponding resolutions ($\theta_{\rm HPBW}$) in milli-arcsecond (mas), which is estimated as $\theta_{\rm HPBW}$ (mas) $\sim 20627 \cdot \lambda$(mm)/B(km).

Table 15: Angular resolutions at each KVN baseline and frequency

Baseline	B (km)	$\theta_{\rm HPBW}$ (mas)			
		22 GHz	43 GHz	86 GHz	129 GHz
KYS–KUS	305.0	9.1	4.7	2.4	1.6
KUS–KTN	358.8	7.8	4.0	2.0	1.3
KTN–KYS	478.0	5.8	3.0	1.5	1.0
KPC–KYS	133.1	20.9	10.8	5.4	3.6
KUS–KPC	232.6	12.0	6.2	3.1	2.0
KTN–KPC	505.8	5.5	2.9	1.4	0.9

3.3 Baseline sensitivity

Table 16 shows sensitivities of the KVN baselines as follow: (1) frequency band, (2) nominal frequency range of KVN receivers, (3) system temperature, (4) typical KVN system-equivalent-flux-density at zenith, (5) antenna gain at the optimal elevation, (6) typical KVN baseline sensitivity for the aggregated recorded data rate of 1024 Mbps, the integration time of 100 sec (K-band), 60 sec (Q-band), and 30 sec (W/D-band), and the bandwidth of 256 MHz, and (7) typical KVN 3-baseline image sensitivity for the on-source integration time of 8 hr.

Table 16: Baseline sensitivity of the KVN

Freq. band	Freq. range (GHz)	$T_{\rm sys}$ (K)	SEFD (mJy)	Gain (K/Jy)	ΔS (mJy)	ΔI (mJy/beam)
(1)	(2)	(3)	(4)	(5)	(6)	(7)
K	21.25–23.25	100	1129	0.089	12	0.2
Q	43.11–44.11	150	1715	0.087	18	0.3
W	85–95	200	2073	0.072	29	0.6
D	125–142	250	3041	0.049	54	1.0

3.4 System temperature

Figure 13 shows seasonal variation of system temperature at each KVN site. The zenith system temperatures corrected for atmospheric attenuation at K-, Q-, W-, and D-bands are presented by four panels from top to bottom, respectively.

3.5 Astrometric observation

Numerous factors (antenna locations, calibrators, timetable, etc.) need to be properly examined and planned to produce accurate astrometric observations. Astrometric VLBI observations using the KVN are not supported at this time. To evaluate the feasibility, we got underway astrometric AGN/Maser test observations; the outcomes will be provided the following year. Please get in touch with us if you wish to make an astrometric observation.

4 Observation and Data Reduction

4.1 Preparation of observation and correlation

4.1.1 General information

For the accepted proposals, the users have to prepare the observing schedule file before the observation. The observer who is not familiar with the KVN system is recommended to consult contact persons of the KVN group to prepare schedules, especially for some observations such as phase referencing, polarimetry, and/or spectral line, etc. The detailed

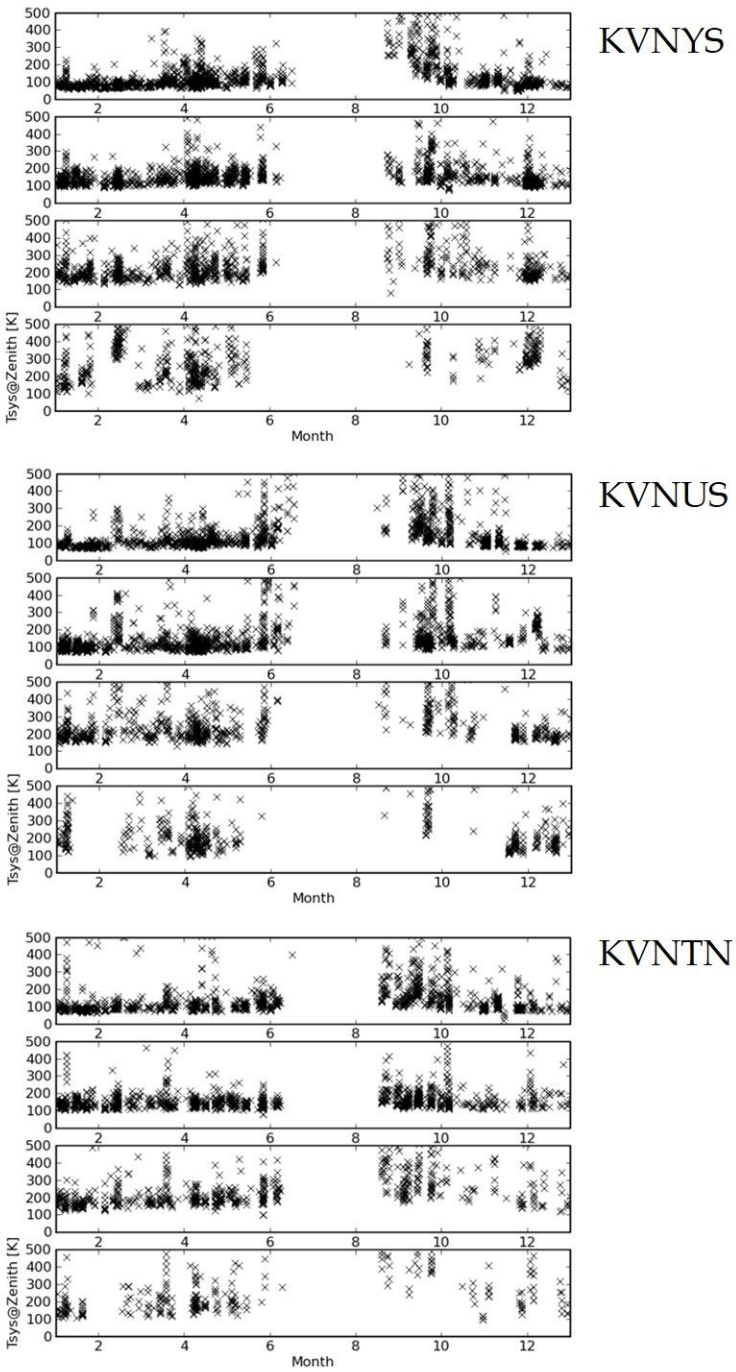

Figure 13: System temperatures of each KVN telescope

information about observation planning and scheduling can be downloaded from the KVN homepage[2].

[2]`https://radio.kasi.re.kr/kvn/user_support.php`

4.1.2 Observation

All KVN experiments should be scheduled using the VEX (VLBI experiment) file. You can either edit and modify the KVN VEX example files or use the VLBA scheduling program SCHED[3]. It is recommended to use SCHED for your scheduling because SCHED provides useful information and many aspects of planning VLBI observations, and you can also avoid many mistakes arising from editing the VEX manually. The user needs to submit the VEX or key files two weeks before the observation. KVN AOC staff will check your schedule and proceed with the observations.

4.1.3 Correlation

Following the observation, the Daejeon correlator or DiFX correlator will perform the correlation procedure in accordance with the parameters that were provided. In order to release and recycle the disk modules and storage used for observation, the user is required to review the correlated data and report if the correlation was correctly performed. If there are any issues, re-correlation may be required. The raw data disk modules utilized for the observations will, in principle, be discarded two months after the correlation. Please see the correlation status report for further details.

4.2 Data reduction

4.2.1 VLBI data reduction with AIPS

Here we introduce a very brief way of reducing VLBI data with KVN (or EAVN). For more detail, please have a look at the data reduction manual[4]. Figure 14 shows one of the procedures for reducing the KVN (or EAVN) observations.

4.3 Correlator status

4.3.1 Daejeon Correlator

Daejeon correlator (KJCC; Korea-Japan Correlation Center) is described in detail on the website[5], so we will not describe the correlator in this report.

4.3.2 Software Correlator

Most KVN observations have been correlated using the DiFX (distributed FX-style) software correlator (see Deller et al. (2007 [8], 2011 [9]). A dedicated computing cluster named "Coma" for software correlation was installed. It is composed of one master and eight computing nodes. The master node has 128 GB of memory and two Intel Xeon E5−2667 v3 processors. Each of the processors has eight cores. Each computing node has 128 GB of memory and two Intel Xeon E5−2698 v4 processors. Each of the processors has 20 cores. The master and computer nodes are connected with 100 Gbps Infiniband and 1 Gbps Ethernet.

[3] http://www.aoc.nrao.edu/~cwalker/sched/sched.html
[4] https://radio.kasi.re.kr/eavn/user_support.php
[5] https://radio.kasi.re.kr/kjcc/main.php

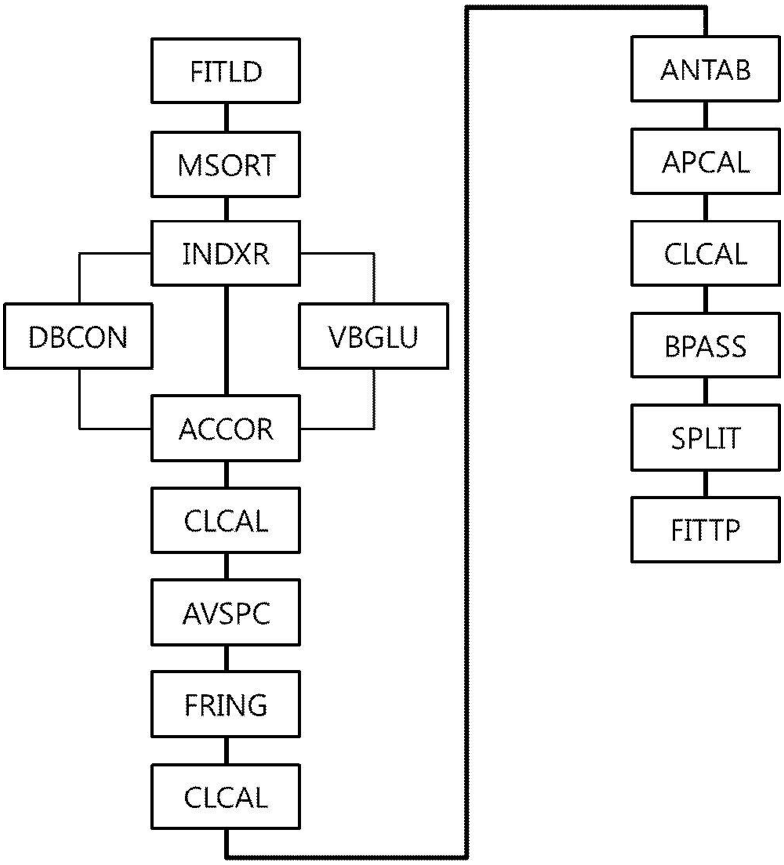

Figure 14: Data reduction flow chart with AIPS

The Infiniband connection is for parallel computation and storage, and the Ethernet connection is for management. OpenHPC has been used to deploy and manage the Coma cluster. A dedicated Lustre file system for the software correlation provides about 3 petabytes. It is connected to the master and each computing node through 100 Gbps Infiniband.

Observation data saved in Mark5b or Mar6 at each KVN site is transported to the Luster file system through the KREONET using GridFTP. The master node has an additional 100 Gbps Ethernet connection to the KREONET. The KYS site is connected to the KREONET using 40 Gbps Ethernet, and the KUS and KTN sites are connected using 10 Gbps.

Figure 15 shows the Coma computing cluster and the Lustre file system. Technical details of the software correlator are described in the website[6].

5 Further information

Contact address It is possible for users to contact any staff member of the KVN by email (see Table 17). The official website[7] also provides various types of information.

[6] http://hpc.kasi.re.kr/difx
[7] http://kvn.kasi.re.kr

Figure 15: A computing cluster and Lustre file system dedicated for the software correlation of the KVN.

Table 17: Contact information

E-mail	Subject
kvnprop@kasi.re.kr	Proposal submission and informing its result
kvnobs@kasi.re.kr	Observing schedule submission, observation-related requests and questions for the accepted proposal only
kjcc@kasi.re.kr	Correlated data distribution and correlation-related requests
kvnhelp@kasi.re.kr	General questions including scheduling, observations, systems, and so on (regardless of the proposal acceptance)

References

[1] S.-S. Lee, L. Petrov, D.-Y. Byun, J. Kim, T. Jung, M.-G. Song, C. S. Oh, D.-G. Roh, D.-H. Je, S.-O. Wi, B. W. Sohn, S.-J. Oh, K.-T. Kim, J.-H. Yeom, M.-H. Chung, J. Kang, S.-T. Han, J.-W. Lee, B. G. Kim, H. Chung, H.-G. Kim, H. Ryoung Kim, Y.-W. Kang, and S.-H. Cho, "Early Science with the Korean VLBI Network: Evaluation of System Performance," *The Astronomical Journal*, vol. 147, p. 77, Apr. 2014.

[2] I. de Pater, R. J. Sault, M. H. Wong, L. N. Fletcher, D. DeBoer, and B. Butler, "Jupiter's ammonia distribution derived from VLA maps at 3-37 GHz," *Icarus*, vol. 322, pp. 168–191, Apr. 2019.

[3] M. Maris, E. Romelli, M. Tomasi, A. Gregorio, M. Sandri, S. Galeotta, D. Tavagnacco, M. Frailis, G. Maggio, and A. Zacchei, "Revised planet brightness temperatures using the Planck/LFI 2018 data release," *Astronomy and Astrophysics*, vol. 647, p. A104, Mar. 2021.

[4] S.-T. Han, J.-W. Lee, J. Kang, D.-H. Je, M.-H. Chung, S.-O. Wi, T. Sasao, and R. Wylde, "Millimeter-wave Receiver Optics for Korean VLBI Network," *International Journal of Infrared and Millimeter Waves*, vol. 29, pp. 69–78, Jan. 2008.

[5] S.-T. Han, J.-W. Lee, J. Kang, C.-S. Oh, D.-Y. Byun, D.-H. Je, M.-H. Chung, S.-O. Wi, M. Song, Y.-W. Kang, S.-S. Lee, S.-Y. Kim, T. Sasao, P. F. Goldsmith, and R. Wylde, "Korean VLBI Network Receiver Optics for Simultaneous Multifrequency Observation: Evaluation," *Publications of the Astronomical Society of the Pacific*, vol. 125, p. 539, May 2013.

[6] L. Petrov, S.-S. Lee, J. Kim, T. Jung, J. Oh, B. W. Sohn, D.-Y. Byun, M.-H. Chung, D.-H. Je, S.-O. Wi, M.-G. Song, J. Kang, S.-T. Han, J.-W. Lee, B. G. Kim, H. Chung, and H.-G. Kim, "Early Science with the Korean VLBI Network: The QCAL-1 43 GHz Calibrator Survey," *The Astronomical Journal*, vol. 144, p. 150, Nov. 2012.

[7] S.-S. Lee, D.-Y. Byun, C. S. Oh, S.-T. Han, D.-H. Je, K.-T. Kim, S.-O. Wi, S.-H. Cho, B. W. Sohn, J. Kim, J. Lee, S.-J. Oh, M.-G. Song, J. Kang, M.-H. Chung, J. A. Lee, J. Oh, J.-H. Bae, S.-Y. Yun, J.-W. Lee, B. G. Kim, H. Chung, D.-G. Roh, C. H. Lee, H. G. Kim, H. Ryoung Kim, J.-H. Yeom, T. Kurayama, T. Jung, P. Park, M. J. Kim, D.-H. Yoon, and W.-J. Kim, "Single-Dish Performance of KVN 21 m Radio Telescopes:

Simultaneous Observations at 22 and 43 GHz," *Publications of the Astronomical Society of the Pacific*, vol. 123, p. 1398, Dec. 2011.

[8] A. T. Deller, S. J. Tingay, M. Bailes, and C. West, "DiFX: A Software Correlator for Very Long Baseline Interferometry Using Multiprocessor Computing Environments," , vol. 119, pp. 318–336, Mar. 2007.

[9] A. T. Deller, W. F. Brisken, C. J. Phillips, J. Morgan, W. Alef, R. Cappallo, E. Middelberg, J. Romney, H. Rottmann, S. J. Tingay, and R. Wayth, "DiFX-2: A More Flexible, Efficient, Robust, and Powerful Software Correlator," , vol. 123, p. 275, Mar. 2011.